Nuclear Science and Techniques (2025) 36:141
https://doi.org/10.1007/s41365-025-01734-z

Constraint on the symmetry energy at high densities from neutron star observations using relativistic mean-field models

Ying Cui[1] · Yuan Tian[1] · Cheng-Jun Xia[2] · Ying-Xun Zhang[1,3] · Zhu-Xia Li[1]

Received: 16 July 2024 / Revised: 25 November 2024 / Accepted: 1 January 2025 / Published online: 3 June 2025

Abstract
In this paper, we constrain the symmetry energy at high densities in nuclear matter using recent observations of neutron stars based on the calculations of relativistic mean-field models. Using the observations of the neutron stars, we obtain the constraint on the symmetry energy at high densities, $S(2\rho_0) = 40.54\pm12.47$ MeV, and $S(3\rho_0) = 44.12\pm29.38$ MeV.

Keywords Equation of state · Symmetry energy · Neutron star

1 Introduction

The nuclear equation of state (EoS), particularly the symmetry energy, is essential in both nuclear physics and astrophysics [1–7]. In nuclear physics, the symmetry energy significantly affects the structure of finite nuclei, including the neutron skin thickness of heavy nuclei [8]. In astrophysics, it influences the key properties of neutron stars, such as their masses and radii [3, 4], as well as their cooling processes [9]. Consequently, constraining the symmetry energy is an important challenge in nuclear physics.

Many experimental attempts have been conducted to constrain the symmetry energy around the saturation density ρ_0 [10–23]. These include measurements of the dipole polarizabilities of ^{208}Pb [14, 15], giant dipole resonance energies [13], isospin diffusion in heavy-ion collisions [11], isobaric analog states [19], and neutron skin thickness [12, 24]. Because of the extensive research on determining the symmetry energy, the constraint on the symmetry energy at saturation density is relatively precise, with a commonly accepted value of $J = 30\pm4$ MeV [10, 11, 13–22].

In contrast, the symmetry energy at suprasaturation remains unclear. Many terrestrial experiments have been performed to extract information on symmetry energy at suprasaturation. In studies on heavy-ion collisions, the constraints on the suprasaturation density dependence of the symmetry energy have been obtained from analyses of the π^-/π^+ ratio [25–31] and n/p elliptic flows ratio [32, 33]. However, the symmetry energy at suprasaturation densities exhibit a large model dependence. This is caused by the difficulties in solving the transport models and extrapolating the finite excited nuclear system to infinite nuclear matter at zero temperature. Consequently, further progress in understanding and constraining the equations of state for nuclear matter at high densities is expected from analyses that incorporate the properties of neutron stars.

The mass measurement of the pulsar PSR J0740+6620 from the Neutron Star Interior Composition

This work was supported by the National Natural Science Foundation of China (Nos. 12275359, 12375129, 11875323, and 11961141003), the National Key R&D Program of China (No. 2023YFA1606402), the Continuous Basic Scientific Research Project, the China Institute of Atomic Energy (Nos. YZ222407001301 and YZ232604001601), the Leading Innovation Project of the CNNC (Nos. LC192209000701 and LC202309000201), and the computing server SCATP in China Institute of Atomic Energy and Basic Research Special Zone.

✉ Ying Cui
yingcuid@163.com

✉ Yuan Tian
tiany@ciae.ac.cn

✉ Ying-Xun Zhang
zhyx@ciae.ac.cn

1 China Institute of Atomic Energy, Beijing 102413, China

2 Center for Gravitation and Cosmology, College of Physical Science and Technology, Yangzhou University, Yangzhou 225009, China

3 Guangxi Key Laboratory Breeding Base of Nuclear Physics and Technology, Guangxi Normal University, Guilin 541004, China

Explorer [34, 35] revealed a neutron star with a mass of $2.08^{+0.07}_{-0.07}\,M_{\odot}$, and GW190814 from the LIGO/Virgo collaboration [36] observed a $2.5-2.67\,M_{\odot}$ compact star because of the neutron stars impose tight constraints on the EoS [37–40]. For the observations of the mass around the 1.4 $M_{\odot}$ neutron star, the analysis of the tidal deformability from GW170817 by LIGO/Virgo [41, 42] along with radius $R_{1.4}=13.02^{+1.24}_{-1.06}$ km and mass–radius posterior distributions from millisecond pulsar PSR J0030+0451 via the (NICER) mission [43] have significantly enhanced the ability to constrain the symmetry energy of nuclear matter [44, 45]. Moreover, constraints on the symmetry energy have been derived from multiple observations of neutron stars in combination with nuclear theory [10, 44–47]. Among these studies, Skyme interactions [45, 48, 49], chiral effective field theory [10] and empirical local density functional metamodels [50] were developed under the non-relativistic framework. Relativistic mean-field models have been widely used to describe the properties of infinite nuclear matter, finite nuclei, and stellar matter [51–54]. A systematically analysis of the influence of all relativistic mean-field (RMF) sets on the properties of neutron stars. In this paper, we utilize RMF models to describe the properties of neutron stars with a focus on exploring the constraints imposed by these models on the EoS and symmetry energy at both saturation and supra-saturation densities.

The remainder of this paper is organized as follows. In Sect. 2, we review the theoretical aspects of RMF models, the EoS of a neutron star, and the Tolman–Oppenheimer–Volkov (TOV) equation. In Sect. 3, we present the results of the constraint on the symmetry energy obtained from the neutron star observations. Finally, the summary is presented in Sect. 4.

2 Model

2.1 Relativistic mean field

In this paper, we employ the framework of RMF models to extract information on the symmetry energy in symmetric nuclear matter (SNM) systems. RMF models provide a comprehensive description of both nuclear matter and finite nuclei and are widely used to study neutron star properties. To better categorize the parametrizations associated with RMF models, Ref. [53] defined three distinct types: (i) nonlinear, (ii) density-dependent, and (iii) point-coupling models.

The Lagrangians for the different RMF models are

1. Nonlinear (NL) model

$$\begin{aligned}\mathcal{L}_{\mathrm{NL}} =&\bar{\Psi}[i\gamma_\mu\partial^\mu - m_{\mathrm{N}}]\Psi + \frac{1}{2}\left(\partial_\mu\sigma\partial^\mu\sigma - m_\sigma^2\sigma^2\right) - U(\sigma)\\ &- \frac{1}{4}\omega_{\mu\nu}\omega^{\mu\nu} + \frac{1}{2}m_\omega^2\omega_\mu\omega^\mu + \frac{1}{4}\zeta^4(\omega_\mu\omega^\mu)^2\\ &- \frac{1}{4}\boldsymbol{\rho}_{\mu\nu}\boldsymbol{\rho}^{\mu\nu} + \frac{1}{2}m_\rho^2\boldsymbol{\rho}_\mu\boldsymbol{\rho}^\mu + \frac{1}{2}\left(\partial_\mu\boldsymbol{\delta}\partial^\mu\boldsymbol{\delta} - m_\delta^2\boldsymbol{\delta}^2\right)\\ &+ g_{\sigma\mathrm{NN}}\bar{\Psi}\Psi\sigma - g_{\omega\mathrm{NN}}\bar{\Psi}\gamma_\mu\Psi\omega^\mu\\ &- g_{\rho\mathrm{NN}}\bar{\Psi}\gamma_\mu\boldsymbol{\tau}\cdot\Psi\boldsymbol{\rho}^\mu + g_{\delta\mathrm{NN}}\bar{\Psi}\boldsymbol{\tau}\cdot\Psi\boldsymbol{\delta}\\ &+ g_\sigma g_\omega^2\sigma\omega_\mu\omega^\mu(\alpha_1 + \frac{1}{2}\alpha_1' g_\sigma)\\ &+ g_\sigma g_\rho^2\sigma\boldsymbol{\rho}_\mu\boldsymbol{\rho}^\mu(\alpha_2 + \frac{1}{2}\alpha_2' g_\sigma)\\ &+ \frac{1}{2}\alpha_3' g_\omega^2 g_\rho^2\omega_\mu\omega^\mu\boldsymbol{\rho}_\mu\boldsymbol{\rho}^\mu.\end{aligned} \tag{1}$$

2. Density dependence (DD) model

$$\begin{aligned}\mathcal{L}_{\mathrm{DD}} =&\bar{\Psi}[i\gamma_\mu\partial^\mu - m_{\mathrm{N}}]\Psi + \frac{1}{2}\left(\partial_\mu\sigma\partial^\mu\sigma - m_\sigma^2\sigma^2\right)\\ &- \frac{1}{4}\omega_{\mu\nu}\omega^{\mu\nu} + \frac{1}{2}m_\omega^2\omega_\mu\omega^\mu - \frac{1}{4}\boldsymbol{\rho}_{\mu\nu}\boldsymbol{\rho}^{\mu\nu} + \frac{1}{2}m_\rho^2\boldsymbol{\rho}_\mu\boldsymbol{\rho}^\mu\\ &+ \frac{1}{2}\left(\partial_\mu\boldsymbol{\delta}\partial^\mu\boldsymbol{\delta} - m_\delta^2\boldsymbol{\delta}^2\right) + \Gamma_\sigma(\rho)\bar{\Psi}\Psi\sigma - \Gamma_\omega(\rho)\bar{\Psi}\gamma_\mu\Psi\omega^\mu\\ &- \Gamma_\rho(\rho)\bar{\Psi}\gamma_\mu\boldsymbol{\tau}\cdot\Psi\boldsymbol{\rho}^\mu + \Gamma_\delta(\rho)\bar{\Psi}\boldsymbol{\tau}\cdot\Psi\boldsymbol{\delta}.\end{aligned} \tag{2}$$

3. Point-coupling (PC) model

$$\begin{aligned}\mathcal{L}_{\mathrm{PC}} =&\bar{\Psi}[i\gamma_\mu\partial^\mu - m_{\mathrm{N}}]\Psi - \frac{\alpha_{\mathrm{S}}}{2}\left(\bar{\Psi}\Psi\right)^2\\ &- \frac{\alpha_{\mathrm{V}}}{2}\left(\bar{\Psi}\gamma_\mu\Psi\right)\left(\bar{\Psi}\gamma^\mu\Psi\right) - \frac{\alpha_{\mathrm{TV}}}{2}\left(\bar{\Psi}\gamma_\mu\boldsymbol{\tau}\Psi\right)\cdot\left(\bar{\Psi}\gamma^\mu\boldsymbol{\tau}\Psi\right)\\ &- \frac{\alpha_{\mathrm{TS}}}{2}\left(\bar{\Psi}\boldsymbol{\tau}\Psi\right)\cdot\left(\bar{\Psi}\boldsymbol{\tau}\Psi\right)\\ &- \frac{\beta_{\mathrm{S}}}{3}\left(\bar{\Psi}\Psi\right)^3 - \frac{\gamma_{\mathrm{S}}}{4}\left(\bar{\Psi}\Psi\right)^4 - \frac{\gamma_{\mathrm{V}}}{4}\left(\bar{\Psi}\gamma_\mu\Psi\bar{\Psi}\gamma^\mu\Psi\right)^2\\ &- \frac{\alpha_{\mathrm{TV}}}{4}\left(\bar{\Psi}\gamma_\mu\boldsymbol{\tau}\Psi\cdot\bar{\Psi}\gamma^\mu\boldsymbol{\tau}\Psi\right)^2\\ &+ [\eta_1 + \eta_2\left(\bar{\Psi}\Psi\right)]\left(\bar{\Psi}\Psi\right)\left(\bar{\Psi}\gamma_\mu\Psi\right)\left(\bar{\Psi}\gamma^\mu\Psi\right)\\ &- \eta_3\left(\bar{\Psi}\Psi\right)\left(\bar{\Psi}\gamma_\mu\boldsymbol{\tau}\Psi\right)\cdot\left(\bar{\Psi}\gamma^\mu\boldsymbol{\tau}\Psi\right),\end{aligned} \tag{3}$$

where $\omega_{\mu\nu}$ and $\boldsymbol{\rho}_{\mu\nu}$ are defined by $\partial_\mu\omega_\nu - \partial_\nu\omega_\mu$ and $\partial_\mu\boldsymbol{\rho}_\nu - \partial_\nu\boldsymbol{\rho}_\mu$, respectively. In Eq.1, $U(\sigma)=\frac{1}{3}g_2\sigma^3+\frac{1}{4}g_3\sigma^4$ is the nonlinear potential of the σ field.

As an example, we use the nonlinear RMF model to present the expressions of relevant quantities [51–53]. In the RMF model, meson fields can be replaced with their expectation values:

$$\begin{aligned}&\sigma \rightarrow <\sigma>=\bar{\sigma},\ \omega^\mu \rightarrow <\omega^\mu>=\bar{\omega}^0\\ &\boldsymbol{\rho}^\mu \rightarrow <\boldsymbol{\rho}^\mu>=\bar{\rho}_3^0,\ \boldsymbol{\delta}^\mu \rightarrow <\boldsymbol{\delta}^\mu>=\bar{\delta}_3^0\end{aligned} \tag{4}$$

The equation of motions (EOMs) for nucleons and mesons were derived from the Lagrangian density:

$$[\gamma^{\mu} i\partial_{\mu} - g_{\omega}\bar{\omega}^0 - g_{\rho}\bar{\rho}_3^0\tau_3 - (m_{\rm N} - g_{\sigma}\bar{\sigma} - g_{\delta}\bar{\delta}_3\tau_3)]\Psi = 0 \quad (5)$$

$$m_{\sigma}^2\bar{\sigma} = g_{\sigma}\rho_{\rm s} - g_2\bar{\sigma}^2 - g_3\bar{\sigma}^3 + g_{\sigma}g_{\omega}^2(\bar{\omega}^0)^2(\alpha_1 + \alpha_1' g_{\sigma}\bar{\sigma}) + g_{\sigma}g_{\rho}^2(\bar{\rho}_3^0)^2(\alpha_2 + \alpha_2' g_{\sigma}\bar{\sigma}) \quad (6)$$

$$m_{\omega}^2\bar{\omega}^0 = g_{\omega}\rho - \zeta g_{\omega}^4(\bar{\omega}^0)^3 - g_{\sigma}g_{\omega}^2\bar{\sigma}\bar{\omega}^0(2\alpha_1 + \alpha_1' g_{\sigma}\bar{\sigma}) - \alpha_3' g_{\omega}^2 g_{\rho}^2(\bar{\rho}_3^0)^2\bar{\omega}^0 \quad (7)$$

$$m_{\rho}^2\bar{\rho}_3^0 = g_{\rho}\rho_3 - g_{\sigma}g_{\rho}^2\bar{\sigma}\bar{\rho}_3^0(2\alpha_2 + \alpha_2' g_{\sigma}\bar{\sigma}) - \alpha_3' g_{\omega}^2 g_{\rho}^2\bar{\rho}_3^0(\bar{\omega}^0)^2 \quad (8)$$

$$m_{\delta}^2\bar{\delta}_3 = g_{\delta}\rho_{\rm s3}, \quad (9)$$

where the different densities are defined as

$$\rho_{\rm s} = \langle\bar{\Psi}\Psi\rangle = \rho_{\rm sn} + \rho_{\rm sp}, \quad (10)$$

$$\rho = \langle\bar{\Psi}\gamma^0\Psi\rangle = \rho_{\rm n} + \rho_{\rm p}, \quad (11)$$

$$\rho_{\rm s3} = \langle\bar{\Psi}\tau_3\Psi\rangle = \rho_{\rm sp} - \rho_{\rm sn}, \quad (12)$$

$$\rho_3 = \langle\bar{\Psi}\gamma^0\tau_3\Psi\rangle = \rho_{\rm p} - \rho_{\rm n}. \quad (13)$$

Filling up to the Fermi momenta $k_{{\rm F},i}$ for $i = $ n or p in the nuclear matter, the neutron (n) and proton (p) scalar and baryon densities are given by

$$\rho_{{\rm s}i} = \frac{C(i)}{(2\pi)^3}\int_{k<k_{{\rm F}i}} d^3\mathbf{k}\frac{m_i^*}{\sqrt{k^2 + m_i^{*2}}} = \frac{m_i^*}{2\pi^2}\left[k_{{\rm F}i}E_{{\rm F}i}^* - m_i^{*2}\ln\frac{k_{{\rm F}i} + E_{{\rm F}i}^*}{m_{\rm i}^{*2}}\right], \quad (14)$$

$$\rho_i = \frac{C(i)}{(2\pi)^3}\int_{k<k_{{\rm F}i}} d^3\mathbf{k} = \frac{(k_{{\rm F}i})^3}{3\pi^2}, \quad (15)$$

where the degeneracy factor $C(i=$n,p$)=2$, and $E_{{\rm F}i}^* = \sqrt{k_{{\rm F}i}^2 + m_i^{*2}}$ is the Fermi energy of neutrons and protons. Here, m_i^* is the Dirac effective mass of nucleons, given by the relation

$$m_{\rm n}^* = m_{\rm N} - g_{\sigma}\bar{\sigma} + g_{\delta}\bar{\delta}_3, \quad (16)$$

$$m_{\rm p}^* = m_{\rm N} - g_{\sigma}\bar{\sigma} - g_{\delta}\bar{\delta}_3. \quad (17)$$

The eigenvalues of the neutrons and protons from the Dirac equation are

$$e_{\rm n} = g_{\omega}\bar{\omega}^0 - g_{\rho}\bar{\rho}_3^0 + \sqrt{k_{\rm n}^{2*} + m_{\rm n}^{*2}}, \quad (18)$$

$$e_{\rm p} = g_{\omega}\bar{\omega}^0 + g_{\rho}\bar{\rho}_3^0 + \sqrt{k_{\rm p}^{2*} + m_{\rm p}^{*2}}. \quad (19)$$

The expressions for the energy density and pressure are obtained from the given Lagrangian using the energy-momentum tensor relation given by

$$T^{\mu\nu} = \sum_i \frac{\partial\mathcal{L}}{\partial(\partial_{\mu}\phi_i)}\partial_{\nu}\phi_i - g^{\mu\nu}\mathcal{L}, \quad (20)$$

where ϕ_i runs over all the possible fields. The energy density ϵ and pressure P can be obtained from the energy-momentum tensor:

$$\begin{aligned}\epsilon_{\rm NL} =& \langle T^{00}\rangle \\ =& \frac{1}{2}m_{\sigma}^2\bar{\sigma}^2 + \frac{1}{3}g_2\bar{\sigma}^3 + \frac{1}{4}g_3\bar{\sigma}^4 - \frac{1}{2}m_{\omega}^2(\bar{\omega}^0)^2 \\ &- \frac{\zeta}{4}g_{\omega}^4(\bar{\omega}^0)^4 + g_{\omega}\bar{\omega}^0\rho - \frac{1}{2}m_{\rho}^2(\bar{\rho}_3^0)^2 + g_{\rho}\bar{\rho}_3^0\rho_3 \\ &+ \frac{1}{2}m_{\delta}^2\bar{\delta}_3^2 - g_{\sigma}g_{\omega}^2\bar{\sigma}(\bar{\omega}^0)^2(\alpha_1 + \frac{1}{2}\alpha_1' g_{\sigma}\bar{\sigma}) \\ &- g_{\sigma}g_{\rho}^2\bar{\sigma}(\bar{\rho}_3^0)^2(\alpha_2 + \frac{1}{2}\alpha_2' g_{\sigma}\bar{\sigma}) - \frac{1}{2}\alpha_3' g_{\omega}^2 g_{\rho}^2(\bar{\rho}_3^0)^2(\bar{\omega}^0)^2 \\ &+ \frac{1}{4}[3E_{\rm F\,n}^*\rho_{\rm n} + m_{\rm n}^*\rho_{\rm s\,n}] + \frac{1}{4}[3E_{\rm F\,p}^*\rho_p + m_{\rm p}^*\rho_{\rm s\,p}],\end{aligned} \quad (21)$$

and

$$\begin{aligned}P_{\rm NL} =& \frac{1}{3}\sum_{i=1}^{3}\langle T^{ii}\rangle \\ =& -\frac{1}{2}m_{\sigma}^2\bar{\sigma}^2 - \frac{1}{3}g_2\bar{\sigma}^3 - \frac{1}{4}g_3\bar{\sigma}^4 \\ &+ \frac{1}{2}m_{\omega}^2(\bar{\omega}^0)^2 + \frac{\zeta}{4}g_{\omega}^4(\bar{\omega}^0)^4 + \frac{1}{2}m_{\rho}^2(\bar{\rho}_3^0)^2 \\ &- \frac{1}{2}m_{\delta}^2\bar{\delta}_3^2 + g_{\sigma}g_{\omega}^2\bar{\sigma}(\bar{\omega}^0)^2(\alpha_1 + \frac{1}{2}\alpha_1' g_{\sigma}\bar{\sigma}) \\ &+ g_{\sigma}g_{\rho}^2\bar{\sigma}(\bar{\rho}_3^0)^2(\alpha_2 + \frac{1}{2}\alpha_2' g_{\sigma}\bar{\sigma}) + \frac{1}{2}\alpha_3' g_{\omega}^2 g_{\rho}^2(\bar{\rho}_3^0)^2(\bar{\omega}^0)^2 \\ &+ \frac{1}{4}[E_{\rm Fn}^*\rho_{\rm n} - m_{\rm n}^*\rho_{\rm sn}] + \frac{1}{4}[E_{\rm Fp}^*\rho_{\rm p} - m_{\rm p}^*\rho_{\rm sp}].\end{aligned} \quad (22)$$

The same calculations for the density dependence and point-coupling models are given in Refs. [55–59].

The binding energy per particle in asymmetric nuclear matter can be expressed as follows:

$$E(\rho,\alpha) = \frac{\epsilon}{\rho} - m_{\rm N} = E_0(\rho) + S(\rho)\alpha^2 + O(\alpha^4). \quad (23)$$

Here, the isoscalar term $E_0(\rho) = E(\rho, \alpha = 0)$ is the binding energy per nucleon in SNM, and the isovector term $S(\rho)$ is the symmetry energy. $\rho = \rho_{\rm n} + \rho_{\rm p}$ is the nuclear matter density, and $\alpha = (\rho_n - \rho_p)/(\rho_n + \rho_p)$ is the isospin asymmetry. The nuclear symmetry energy $S(\rho)$ is defined as

$$S(\rho) = \frac{1}{2}\frac{\partial^2 E(\rho,\alpha)}{\partial\alpha^2}\ |_{\alpha=0}\ . \tag{24}$$

The symmetry energy is expanded in terms of $(\rho - \rho_0)/3\rho_0$ as

$$S(\rho) = J + \frac{L}{3\rho_0}(\rho - \rho_0) + \cdots, \tag{25}$$

where $J = S(\rho_0)$ is the symmetry energy, and $L = 3\rho_0 \frac{\partial S}{\partial\rho}\ |_{\rho=\rho_0}$ is the slope of the symmetry energy at the saturation density.

For SNM, $m_n^* = m_p^* = m_N^*$ because $\bar{\delta}_3$ vanishes. The symmetry energies of the RMF models are expressed as follows:

$$S(\rho)_{NL} = \frac{k_F^2}{6E_F^*} + \frac{1}{2}\rho\frac{g_\rho^2}{m_\rho^{*2}} - \frac{1}{2}\rho\left(\frac{\frac{g_\delta^2}{m_\delta^2}m_N^{*2}}{E_F^{*2}[1+\frac{g_\delta^2}{m_\delta^2}A(\rho,m_N^*)]}\right), \tag{26}$$

$$S(\rho)_{DD} = \frac{k_F^2}{6E_F^*} + \frac{1}{2}\rho\frac{\Gamma_\rho^2}{m_\rho^2} - \frac{1}{2}\rho\left(\frac{\frac{\Gamma_\delta^2}{m_\delta^2}m_N^{*2}}{E_F^{*2}[1+\frac{\Gamma_\delta^2}{m_\delta^2}A(\rho,m_N^*)]}\right), \tag{27}$$

$$\begin{aligned} S(\rho)_{PC} = &\frac{k_F^2}{6E_F^*} + \frac{1}{2}\alpha_V\rho + \eta_3\rho_s\rho \\ &+ \frac{1}{2}\alpha_{TS}\rho\left(\frac{m_N^{*2}}{E_F^{*2}[1-\alpha_{TS}A(\rho,m_N^*)]}\right), \end{aligned} \tag{28}$$

where $m_\rho^{*2} = m_\rho^2 + g_\sigma g_\rho^2\bar{\sigma}(2\alpha_2 + \alpha_2' g_\sigma\bar{\sigma}) + \alpha_3' g_\omega^2 g_\rho^2(\bar{\omega}^0)^2$, and

$$A(\rho, m_N^*) = 3\left(\frac{\rho_s}{m_N^*} - \frac{\rho}{E_F^*}\right). \tag{29}$$

The expressions of the slope of symmetry energy (L) of the various RMF models are

$$\begin{aligned} L_{NL} =&\frac{k_F^2}{3E_F^*}\left(1 - \frac{k_F^2}{2E_F^{*2}} - \frac{k_F^3 m_N^*}{E_F^{*2}\pi^2}\frac{\partial m_N^*}{\partial\rho}\right) \\ &+ \frac{3g_\rho^2}{2m_\rho^{*2}}\rho\left(1 - \frac{1}{m_\rho^{*2}}\frac{\partial m_\rho^{*2}}{\partial\rho}\rho\right) \\ &- \frac{1}{2}\rho\left(\frac{\frac{g_\delta^2}{m_\delta^2}m_N^{*2}}{E_F^{*2}[1+\frac{g_\delta^2}{m_\delta^2}A(\rho,m_N^*)]}\right) \\ &\times\left\{3 - \frac{2k_F^2}{E_F^{*2}} + 6\left(1 - \frac{m_N^{*2}}{E_F^{*2}}\right)\frac{\rho}{m_N^*}\frac{\partial m_N^*}{\partial\rho}\right. \\ &- 3\frac{g_\delta^2}{m_\delta^2}\frac{1}{1+\frac{g_\delta^2}{m_\delta^2}A}\left[2A\left(\frac{\rho}{m_N^*}\frac{\partial m_N^*}{\partial\rho}\right)\right. \\ &\left.\left.+ \rho\frac{k_F^2}{E_F^{*3}}\left(1 - 3\frac{\rho}{m_N^*}\frac{\partial m_N^*}{\partial\rho}\right)\right]\right\}, \end{aligned} \tag{30}$$

$$\begin{aligned} L_{DD} =&\frac{k_F^2}{3E_F^*}\left(1 - \frac{k_F^2}{2E_F^{*2}} - \frac{k_F^3 m_N^*}{E_F^{*2}\pi^2}\frac{\partial m_N^*}{\partial\rho}\right) \\ &+ \frac{3\Gamma_\rho^2}{2m_\rho^2}\rho\left(1 + 6\frac{\rho}{\Gamma_\rho}\frac{\partial\Gamma_\rho}{\partial\rho}\right) \\ &- \frac{1}{2}\rho\left(\frac{\frac{\Gamma_\delta^2}{m_\delta^2}m_N^{*2}}{E_F^{*2}\left[1+\frac{\Gamma_\delta^2}{m_\delta^2}A(\rho,m_N^*)\right]}\right) \\ &\times\left\{3 + 6\frac{\rho}{\Gamma_\delta}\frac{\partial\Gamma_\delta}{\partial\rho} - \frac{2k_F^2}{E_F^{*2}} + 6\left(1 - \frac{m_N^{*2}}{E_F^{*2}}\right)\frac{\rho}{m_N^*}\frac{\partial m_N^*}{\partial\rho}\right. \\ &- 3\frac{\Gamma_\delta^2}{m_\delta^2}\frac{1}{1+\frac{\Gamma_\delta^2}{m_\delta^2}A}\left[2A\left(\frac{\rho}{\Gamma_\delta}\frac{\partial\Gamma_\delta}{\partial\rho} + \frac{\rho}{m_N^*}\frac{\partial m_N^*}{\partial\rho}\right)\right. \\ &\left.\left.+ \rho\frac{k_F^2}{E_F^{*3}}\left(1 - 3\frac{\rho}{m_N^*}\frac{\partial m_N^*}{\partial\rho}\right)\right]\right\}, \end{aligned} \tag{31}$$

$$\begin{aligned} L_{\rm PC} =& \frac{k_{\rm F}^2}{3E_{\rm F}^*}\left(1-\frac{k_{\rm F}^2}{2E_{\rm F}^{*2}}-\frac{k_{\rm F}^3 m_{\rm N}^*}{E_{\rm F}^{*2}\pi^2}\frac{\partial m_{\rm N}^*}{\partial\rho}\right)\\ &+\frac{3}{2}\alpha_{\rm V}\rho+3\eta_3\rho_{\rm s}\rho+3\eta_3\rho^2\frac{\partial\rho_{\rm s}}{\partial\rho}\\ &+\frac{1}{2}\alpha_{\rm TS}\rho\left(\frac{m_{\rm N}^{*2}}{E_{\rm F}^{*2}[1-\alpha_{\rm TS}A(\rho,m_{\rm N}^*)]}\right)\\ &\times\left\{3-\frac{2k_{\rm F}^2}{E_{\rm F}^{*2}}+6\left(1-\frac{m_{\rm N}^{*2}}{E_{\rm F}^{*2}}\right)\frac{\rho}{m_{\rm N}^*}\frac{\partial m_{\rm N}^*}{\partial\rho}\right.\\ &+3\alpha_{\rm TS}\frac{1}{1-\alpha_{\rm TS}A}\left[2A\left(\frac{\rho}{m_{\rm N}^*}\frac{\partial m_{\rm N}^*}{\partial\rho}\right)\right.\\ &\left.\left.+\rho\frac{k_{\rm F}^2}{E_{\rm F}^{*3}}\left(1-3\frac{\rho}{m_{\rm N}^*}\frac{\partial m_{\rm N}^*}{\partial\rho}\right)\right]\right\}. \end{aligned} \tag{32}$$

In this paper, we utilize 180 interaction parameter sets selected from those used in RMF models [53]. These parameter sets satisfy the incompressibility at saturation densities K_0 within the range of 200 to 300 A MeV by computing the distribution of isoscalar monopole strength in ^{208}Pb with relativistic models [60]. The interaction parameter sets are listed below, and detailed information is available in Ref. [53]:

(i)165 nonlinear RMF models (E [61], ER [61], NL1 [51], NL3 [62], NL3-II [62], NL3* [63], NL4 [64], NLC [54], NLB1 [51], NLB2 [51], NLRA1 [65], NLS [66], P-067 [67], P-070 [67], P-075 [67], P-080 [67], GL1 [68], GL2 [68], GL3 [68], GL4 [68], GL5 [68], GL6 [68], GL7 [68], GL8 [68], GL82 [69], GL9 [68], GM1 [70], GM2 [70], GM3 [70], GPSa [71], GPSb [71], NLρA [72], NLρB [72], RMF301 [73], RMF302 [73], RMF303 [73], RMF304 [73], RMF305 [73], RMF306 [73], RMF307 [73], RMF308 [73], RMF309 [73], RMF310 [73], RMF311 [73], RMF312 [73], RMF313 [73], RMF314 [73], RMF315 [73], RMF316 [73], RMF317 [73], RMF401 [73], RMF402 [73], RMF403 [73], RMF404 [73], RMF405 [73], RMF406 [73], RMF407 [73], RMF408 [73], RMF409 [73], RMF410 [73], RMF411 [73], RMF412 [73], RMF413 [73], RMF414 [73], RMF415 [73], RMF416 [73], RMF417 [73], RMF418 [73], RMF419 [73], RMF420 [73], RMF421 [73], RMF422 [73], RMF423 [73], RMF424 [73], RMF425 [73], RMF426 [73], RMF427 [73], RMF428 [73], RMF429 [73], RMF430 [73], RMF431 [73], RMF432 [73], RMF433 [73], RMF434 [73], Q1 [74], G1 [74], G2 [74], SMFT2 [75], DJM [75], S271 [76], Z271 [76], SRK3M5 [77], HD [78],HC [78], MS1 [79], MS3 [80], XS [80], NLSV1 [81], NLSV2 [81], TM1 [82], PK1 [83], hybrid [84], Z271* [85], G2* [85], BKA20 [86], BKA22 [86], BKA24 [86], FSUGOLD [9], FSUGOLD4 [87], FSUGOLD5 [87], FSUGZ00 [88], FSUGZ03 [88], FSUGZ06 [88], IU-FSU [89], NL3V1 [90], NL3V2 [90], NL3V3 [90], NL3V4 [90], NL3V5 [90], NL3V6 [90], S271V1 [90], S271V2 [90], S271V3 [90], S271V4 [90], S271V5 [90], S271V6 [90], Z271S1 [90], Z271S2 [90], Z271S3 [90], Z271S4 [90], Z271S5 [90], Z271S6 [90], Z271V1 [90], Z271V2 [90], Z271V3 [90], Z271V4 [90], Z271V5 [90], Z271V6 [90], TM1* [91], BSR1 [92], BSR2 [92], BSR3 [92], BSR4 [92], BSR5 [92], BSR6 [92], BSR7 [92], BSR8 [92], BSR9 [92], BSR10 [92], BSR11 [92], BSR12 [92], BSR13 [92], BSR14 [92], BSR15 [92], BSR16 [92], BSR17 [92], BSR18 [92], BSR19 [92], BSR20 [92], BSR21 [92], SVI-1 [93], SVI-2 [93], SIG-OM [94], NL$\rho\delta$ A [72], NL$\rho\delta$B [72]);

(ii) Nine density-dependent RMF models (TW99 [95],DD-ME1 [96],PKDD [83], DD-ME2 [58], DD [97], DD-F [98], DD2 [99], DDMEδ [59], DDRH$\rho\delta$ [59]);

(iii)6 point-coupling RMF models (FA3 [57], FA4 [57], FZ3 [57], VZ3 [57], PC-F1 [55], PC-F3 [55]).

2.2 Equation of state of a neutron star

For different density regions of a neutron star, different forms of the EoS are employed in this paper as follows.

(i) For the outer crust of a neutron star, the EoS provided by Baym, Pethick, and Sutherland (BPS) [100] is adopted for densities in the range $\rho_{\rm min} \le \rho \le \rho_{\rm outer}$. Here, $\rho_{\rm min}$ is the minimum density ($\rho_{\rm min}$ =4.73×10^{-15} fm^{-3}), with the corresponding energy density $\epsilon_{\rm min}$=4.38×10^{-12} MeV fm^{-3} and pressure $P_{\rm min}$= 6.3×10^{-25} MeV fm^{-3}. The outer crust density is $\rho_{\rm outer}$=2.57×10^{-4} fm^{-3} with an energy density $\epsilon_{\rm outer}=0.24$ MeV fm^{-3}and pressure $P_{\rm outer}$ =4.86×10^{-4} MeV fm^{-3}. In this region, because of the heavy nuclei, primarily around the iron mass number, a Coulomb lattice coexists in β-equilibrium (i.e., equilibrium with respect to weak interaction processes) with an electron gas in the neutron star outer crust [100].

(ii) For the inner crust, $\rho_{\rm outer} < \rho \le \rho_{\rm T}$, the EoS takes the form $P = A + B\epsilon^{4/3}$ from Refs. [101, 102], where two constants A and B are adjusted to match the outer crust EoS to that of a liquid core at the crust–core transition density $\rho_{\rm T}$ ($\rho_{\rm T} = 0.5\rho_0$ [103]).

(iii) In the liquid core region, also referred to as the outer core (OC) region, the density range is $\rho_{\rm T} < \rho \le \rho_{\rm OC}$ ($\rho_{\rm OC} = 3\rho_0$), where the EOS is obtained using the RMF. This region requires the system to be in β-equilibrium and is composed of protons, neutrons, electrons, and muons. For β equilibrium to be attained in nuclear matter, the following electroweak processes must occur: $\mathrm{n} \to \mathrm{p} + \mathrm{e}^- + \bar{\nu}_{\rm e}$, $\mathrm{p} + \mathrm{e}^- \to \mathrm{n} + \nu_{\rm e}$, $\mathrm{e}^- \to \mu^- + \nu_{\rm e} + \bar{\nu}_\mu$, $\mathrm{p} + \mu^- \to \mathrm{n} + \nu_\mu$, and $\mathrm{n} \to \mathrm{p} + \mu^- + \nu_\mu$. The β-equilibrated matter must satisfy the following conditions for the chemical potentials:

$$\mu_{\rm n} - \mu_{\rm p} = \mu_{\rm e},\ \ \mu_{\rm e} = \mu_\mu, \tag{33}$$

where $\mu_{\nu_i} = 0, i = \mathrm{e}, \mu$. At zero temperature, the neutron and proton chemical potentials are $\mu_n = e_n$ and $\mu_p = e_p$, respectively. For relativistic degenerate electrons,

$$\mu_e = \sqrt{m_e^2 + k_{Fe}^2} = \sqrt{m_e^2 + (3\pi^2 x_e \rho)^{2/3}}, \tag{34}$$

$$\mu_\mu = \sqrt{m_\mu^2 + k_{F\mu}^2} = \sqrt{m_\mu^2 + (3\pi^2 x_\mu \rho)^{2/3}}, \tag{35}$$

where m_e =0.511 MeV, and m_μ =0.105 GeV. With the particle fraction $x_i = \rho_i/\rho$ $(i = \mathrm{n, p, e}, \mu)$, $x_p = x_e + x_\mu$ satisfies charge neutrality.

(iv) For the neutron star inner core (IC) region at a high density ($\rho > \rho_{OC}$), studies have incorporated exotic particles such as hyperons, Δs, quarks, and dark matter into the core of massive neutron stars at densities exceeding $3\rho_0$ [104–115]. However, owing to the significant uncertainties in the interactions between nucleons and exotic particles (e.g., hyperons, Δs, and quarks), and the unclear composition of the neutron star core, a polytropic EoS is employed instead of explicitly modeling all possible exotic particles. In this paper, a piecewise polytropic EoS of the form $P_i(\rho) = \kappa_i \rho^{\gamma_i}$ [116–118] is used to smoothly extend the EoS to the density region of the IC of the neutron star ($\rho > \rho_{OC}$). The polytropic EoS is constructed as follows:

$$P_i = \kappa_i \rho^{\gamma_i}, \quad \text{with } \kappa_i \approx \kappa_{i-1} \tag{36}$$

$$\gamma_i = \frac{\ln(P_i/P_{i-1})}{\ln(\rho_i/\rho_{i-1})}, \quad P_i = P_{i-1}\left(\frac{\rho_i}{\rho_{i-1}}\right)^{\gamma_i}, \tag{37}$$

$$\epsilon_i = \left(\epsilon_{i-1} - \frac{P_{i-1}}{\gamma_i - 1}\right)\left(\frac{P_i}{P_{i-1}}\right)^{1/\gamma_i} + \frac{P_i}{\gamma_i - 1}, \tag{38}$$

where the set of dividing densities $\rho_{OC} = \rho_1 < \rho_2 < \cdots$, and $\rho_{i+1} - \rho_i = \Delta\rho = 0.05\rho_0$.

In summary, the EoS of neutron star matter is

$$P(\epsilon) = \begin{cases} P_{BPS}(\epsilon) & \text{for } \rho_{min} \le \rho \le \rho_{outer} \\ A + B\epsilon^{4/3} & \text{for } \rho_{outer} < \rho \le \rho_T \\ P_{RMF}(\epsilon) & \text{for } \rho_T < \rho \le \rho_{OC} \\ P_{IC}(\epsilon) & \text{for } \rho > \rho_{OC}, \end{cases}$$

where $P = P_N + P_e + P_\mu$, $\epsilon = \epsilon_N + \epsilon_e + \epsilon_\mu$, and the total pressure and energy density should include the leptons. The thermodynamically stable EoS must satisfy $\frac{\partial P}{\partial \epsilon} \ge 0$. The adiabatic speed of sound can be expressed as

$$c_s^2 = \left(\frac{v_s}{c}\right)^2 = \frac{\partial P}{\partial \epsilon} < 1, \tag{39}$$

where ϵ is the energy density of the β-stable nuclear matter. For the causality condition, i.e., the speed of sound is always less than that of light $v_s < c$.

2.3 Tolman–Oppenheimer–Volkov equation

The structure of a neutron star is obtained by solving the TOV equation derived from General Relativity [119–121]. The TOV equations are

$$\frac{dP}{dr} = -\frac{GM\epsilon}{r^2}\frac{(1 + P/\epsilon)(1 + 4\pi r^3 P/M)}{1 - 2GM/r}, \tag{40}$$

$$\frac{dM}{dr} = 4\pi r^2 \epsilon, \tag{41}$$

where G=6.707 × 10^{-45} MeV^{-2} is the gravitational constant, r is the distance from the core of the star, $P = P(r)$ is the pressure, and $M = M(r)$ is the mass with radius r.

The in-spiral phase of the two merging neutron stars creates strong tidal gravitational fields, resulting in the deformation of the multipolar structure of the star. The deforming effects are quantified through the tidal deformability parameter Λ, which relates the induced mass quadruple moment $\mathcal{Q}_{ij}$ to the time-independent external tidal field $\mathcal{E}_{ij}$ through the relation [122–124]:

$$\mathcal{Q}_{ij} = -k_2 \frac{2R^5}{3G}\mathcal{E}_{ij}. \tag{42}$$

Here, k_2 is the Love number, which can be obtained from the solution of the first-order differential equation [124]

$$\frac{dy}{dr} = -\frac{y^2}{r} - \frac{y}{r}\frac{(r - 4\pi G r^3(\epsilon - p))}{r - 2GM} - rQ, \tag{43}$$

$$Q = \frac{4\pi r\left[G\left(5\epsilon + 9p + (\epsilon + p)/c_s^2\right) - \frac{3}{2}\frac{1}{\pi r^2}\right]}{1 - 2GM/r} - \left[\frac{2G(M + 4\pi p r^3)}{r(r - 2GM)}\right]^2, \tag{44}$$

$$\begin{aligned} k_2 = &\frac{8}{5}\beta^5(1 - 2\beta)^2[2 - y_R + 2\beta(y_R - 1)] \\ &\times \{2\beta[6 - 3y_R + 3\beta(5y_R - 8)] \\ &+ 4\beta^3[13 - 11y_R + \beta(3y_R - 2) + 2\beta^2(1 + y_R)] \\ &+ 3(1 - 2\beta)^2[2 - y_R + 2\beta(y_R - 1)]\ln(1 - 2\beta)\}^{-1}, \end{aligned} \tag{45}$$

where $y_R = y(R)$, and $\beta = GM/R$. Eqs. 40, 41, 43 are solved using the boundary conditions at the center of the star, $M(0)$ =0, $P(0) = P_c$, and $y(0)$ =2, where P_c is the central pressure. Varying P_c yields all possible stars for a given EoS. Thus, $P(R)$ =0 (vacuum pressure being set to zero) defines the radius of star R and the total gravitational mass of the star is $M(R)$, which is simply denoted by M in the following.

The dimensionless deformability Λ is defined as follows:

$$\Lambda = \frac{2k_2}{3}\left(\frac{R}{GM}\right)^5 . \quad (46)$$

3 Results and discussions

Generally, most RMF models are adjusted to describe nuclei and nuclear matter in the density region from near subsaturation density $\rho \approx 2/3\rho_0$ (average between central and surface densities [76, 103, 125–128]) to saturation density. Moreover, the symmetry energy has large variations at high densities obtained using different parameters of RMF models. The symmetry energy as a function of density obtained by RMF models with 180 parameter sets is shown in Fig. 1.

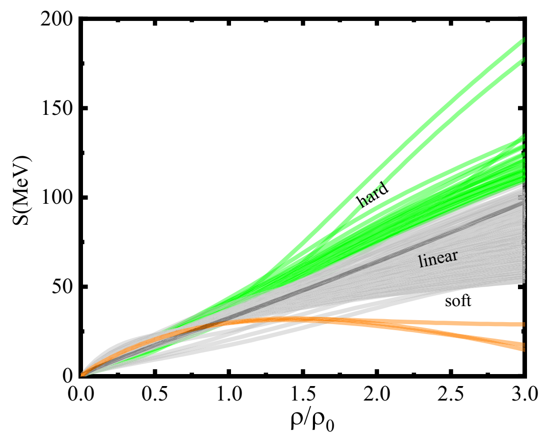

Fig. 1 (Color online) Symmetry energy for 180 RMF models as a function of density ρ/ρ_0; the green, gray, and orange lines represent hard, linear, and soft symmetry energies, respectively

We observe that various RMF models predict very different density behaviors of the symmetry energy, particularly at suprasaturation densities $\rho > \rho_0$. For example, the magnitude of the symmetry energy varies from 29.5 to 114.8 MeV at $2\rho_0$ and from about 14.7 to 188.7 MeV at a density of $3\rho_0$. In Fig. 1, the symmetry energy behaviors are classified into three types: hard, linear, and soft, represented by the green, gray, and orange lines, respectively. We observe from the figure that most of the symmetry energy occurs near the linear types in RMF models.

In this paper, we use the observations of neutron stars to constrain the nuclear EoS at high densities $\rho \geq \rho_0$ because neutron star properties are strongly correlated with the nuclear EoS, as mentioned in Ref. [44, 50, 129]. This constraint can be obtained from the measurements of neutron stars for a mass of $M = 1.4\ M_{\odot}$, such as the tidal deformability from the analysis of gravitational wave data, $\Lambda_{1.4} \approx 190^{+390}_{-120}$ from GW170817 [41], and the radius–mass relation from both GW170817 and PSRJ0030+0451 [41, 43]. For the maximum masses of neutron stars, the maximum neutron star mass $M^{\mathrm{Max}} \geq 2\ M_{\odot}$ is used from Refs. [35, 42], because a compact star with a mass of $2.59^{+0.08}_{-0.09}\ M_{\odot}$ may be the lightest black hole [36].

Our results for tidal deformability with the empirical values from GW170817 (red point) [41] are plotted in panel (a) of Fig. 2. The mass–radius relationship of neutron stars is shown in panel (b) of Fig. 2, where the pink shaded areas represent the region of the posterior distributions at 90% confidence the analysis from PSRJ0030+0451 [43], the blue shaded region is the posterior distribution at 95.4% confidence from PSR J0740+6620 [39], and the purple and green shaded areas denote the region of the posterior distributions at 90% confidence for GW170817's lighter and heavier neutron stars [42],

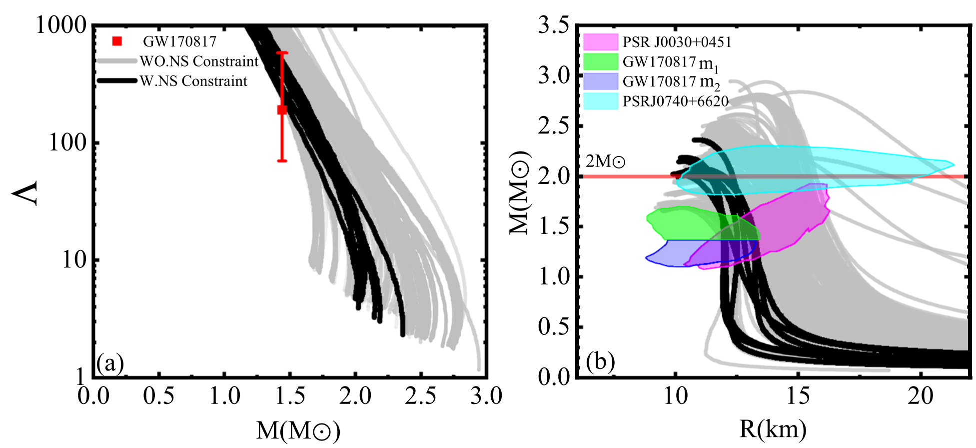

Fig. 2 (Color online) **a** Tidal deformability Λ as a function of the neutron star mass M, where the gray and black lines are the results from the RMF models without and with constraint of the neutron star, respectively. **b** Neutron star mass M as a function of neutron star radius R. The green, purple, and pink shaded regions are the posterior distributions at 90% confidence for GW170817's lighter neutron star, GW170817's heavier neutron star [42], and J0030+0451 [43], respectively. The blue shade region represents the posterior distributions at 95.4% confidence from PSR J0740+6620 [39]

respectively. In Fig. 2, the gray lines represent the results for all the selected 180 RMF parameter sets, which are models without the constraint of the neutron star. With the constraint from the observables of neutron stars such as tidal deformability [41] and mass–radius relation around 1.4 $M_\odot$ [42, 43] combined with the maximum masses of neutron stars above $2M_\odot$, the results of restricted RMF models are indicated by black lines in Fig. 2. Because of the neutron star multi-observables, the analysis of empirical values excludes most RMF parameter sets, and only nine sets remain: HC, FSUGZ03, IU-FSU, G2*, BSR8, BSR9, DD-F, FA3, and FZ3, which can simultaneously describe both the tidal deformability [41] and the overlap of the two mass–radius relation regions [42, 43]. The symmetry energy for RMF models HC, FSUGZ03, IU-FSU, G2*, BSR8, BSR9 is described by Eq. 27, that for DD-F by Eq. 28, and that for FA3, FZ3 by Eq. 28.

Figure 3 shows a comparison of the pressure–density relations between the empirical values from measurements of neutron stars and the RMF model calculations. The green shaded regions enclose the empirical pressure given by the "spectral" EoS inferred from the Bayesian analysis of the GW170817 data at a 90% confidence level, maintaining the lower limit of the maximum neutron star mass at 2 $M_\odot$. Our results of the pressure–density relation (black lines) for neutron-rich matter with β stability are mostly under the limit of the empirical region at the OC ($0.5\rho_0 < \rho \le 3\rho_0$), where the EoS is described by RMF models. For the IC area, $\rho > 3\rho_0$, the order-by-order polytropes EoS in Eqs. (36, 37, 38) occur primarily in the region of neutron star measurement (except the EoS from the HC model).

Figure 4 depicts the constraints on the $J-L$ relation, which were compiled in [10, 130, 131]. In this paper, the symmetry energy $J-L$ constraint from the neutron star observables based on the RMF models is shown as scattering points (cyan stars) with the range of symmetry energy at saturation $J = 30.66\pm0.96$ MeV, and slope $L = 49.47\pm20.39$ MeV. Figure 4 includes the $J-L$ constraints obtained in the analysis of the finite nuclei (neutron skin thicknesses of Sn isotopes and ^{209}Pb, isobaric analog states and isovector skins, and the dipole polarizability of ^{209}Pb) and nuclear matter (heavy-ion collisions and chiral effective field theory calculations of nuclear matter). The enclosed overlap region [131] from constraints obtained from experimental measurements of the neutron skin thicknesses of Sn, dipole polarizabilities, giant dipole resonances, heavy-ion collisions, and nuclear mass fitting correspond to J of approximately 29.0–32.7 MeV, and L is approximately 40.5– 61.9 MeV [130, 131]. In this paper, the constraints for the symmetry energy and its slope at saturation, which are obtained from neutron star observables, are almost in this overlap region, as shown in Fig. 4. Our results can reproduce the properties of neutron stars but cannot reproduce the PREX-II neutron skin using the RMF model. Compared with the research by Chen et al. [132], where the slope parameter $L = 80\pm25$ MeV was obtained from a study of 23 RMF parameter sets, the result in this paper, $L = 49.47\pm20.39$ MeV, is relatively soft.

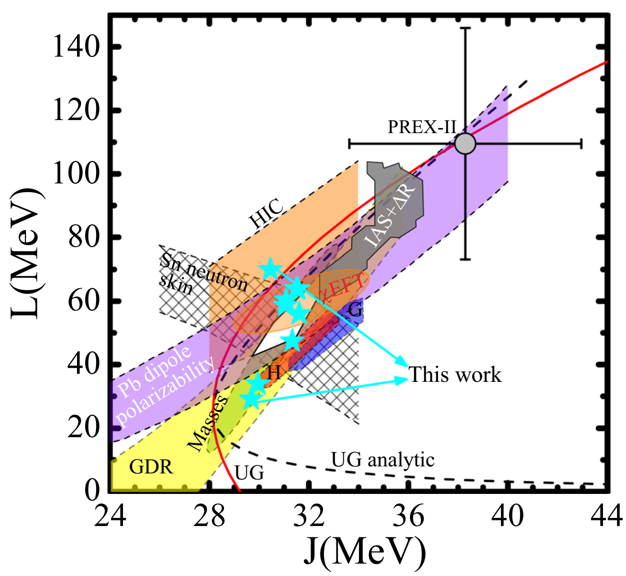

Fig. 4 (Color online) Constraints on the $J-L$ correlation. The cyan stars are our result with the constraint from the RMF models using the neutron star observables. The enclosed white area is the overlap region obtained from heavy-ion collisions (HIC) [11], neutron skin thicknesses of Sn isotopes [12], giant dipole resonances (GDR) [13], the dipole polarizability of ^{208}Pb [14, 15], and the energy density functionals for nuclear masses (masses) [16]. Experimental constraints are obtained from the isobaric analog states and isovector skins (IAS+ΔR) [19], unitary gas (UG) limit by Tews et al. [22], and the neutron skin thicknesses of ^{208}Pb [24]. The microscopic calculations of neutron matter have shown to be χEFT are from chiral effective field theory via the Gaussian Process–BUQEYE collaboration [10], Hebeler et al. (H) [20], and Gandolfi et al. (G) [21]

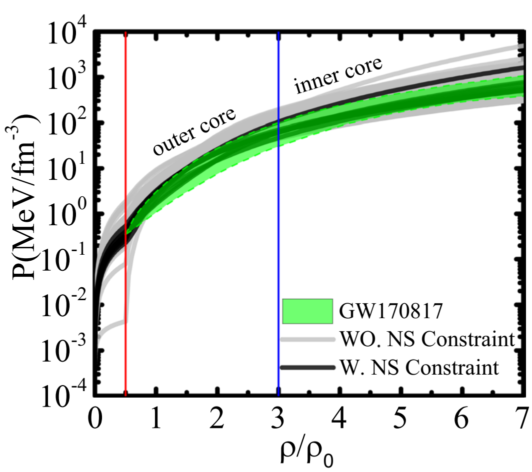

Fig. 3 (Color online) Pressure as a function of density for the neutron-rich matter with β stability. The green shaded area represents data from GW170817 [42]

The symmetry energy at $\rho_0 \leq \rho \leq 3\rho_0$ constrained using the neutron star multi-observables is displayed as a cyan shaded region in Fig. 5. Analysis of doubly magic nuclei and masses of neutron-rich nuclei [133] (black square), isobaric analog states (IAS) [134] (red region), and isospin diffusion in heavy-ion collisions [11] (olive region), the electric dipole polarizability in ^{209}Pb [135] (red point), the multi-observables (isospin diffusion, neutron skin and neutron star) [45] (blue dash line), χEFT (magenta hatched) based on Gaussian Process–BUQEYE (χEFT-GPB) Collaboration [10, 136, 137], the constraint from neutron star observations and nuclear matter experiments (gray hatched shaded area) [47], and neutron skin thicknesses of ^{209}Pb by PREX-II [24] (up triangle), are also included for comparison. To obtain full information on the symmetry energy, we also present the range of symmetry energies at suprasaturation $S(2\rho_0)$ = 28.07–53.00 MeV, and $S(3\rho_0)$ = 14.74–73.49 MeV in Fig.5. Our result for the symmetry energy constraint is similar to that from the χEFT-GPB Collaboration, which is a microscopic calculation. The symmetry energy at a high density in this paper is softer than the result from Tsang et al. [47] (gray hatched area), which used parametric priors based on an expansion that is widely used in nuclear physics. This discrepancy suggests that further constraints on the symmetry energy should be achieved by reducing the uncertainties in the HIC experiments. Additionally, the pressure of the SNM is presented in Appendix.A.

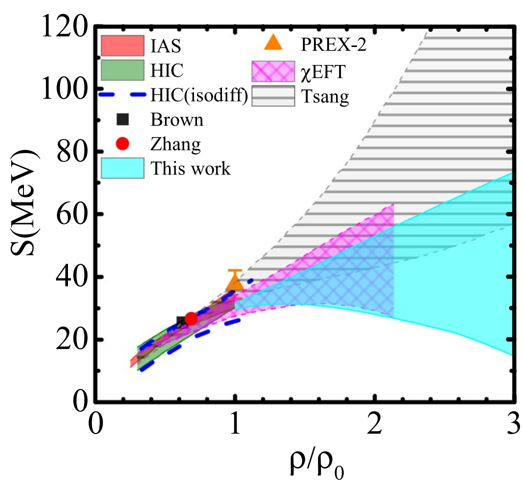

Fig. 5 (Color online) Symmetry energy as a function of density. The blue shadowed region represents the symmetry energy constraint by the observables of the neutron star in this paper. The black square shows the properties of doubly magic nuclei (DMN) and masses of neutron-rich nuclei [133], the red region represents results of IAS [134], the olive region is from HIC [11], the red point is from the electric dipole polarizability (EDP) in ^{209}Pb [135], the blue dash line represents data obtained using multi-observables (isospin diffusion, neutron skin and neutron star) [45], the magenta (hatched) contours represent the calculations from χEFT based on the Gaussian process from the BUQEYE Collaboration [10, 136, 137], the gray (hatched) shaded area shows the constraint from neutron star observations and nuclear matter (NSNM) experiments [47], and, for the neutron, the triangle shows constraints from neutron skin thicknesses of ^{209}Pb by PREX-II

4 Summary

We have extracted information on the symmetry energy at suprasaturation densities from astronomical observations using relativistic mean-field models. In this paper, we have employed 180 RMF parameter sets with incompressibility at the saturation density K_0 =200– 300 MeV, which are suitable for describing the isoscalar monopole distribution strength in ^{209}Pb. By combining the measurements of the 1.4 solar-mass neutron stars, such as tidal deformability ($\Lambda_{1.4} \approx 190^{+390}_{-120}$), the mass–radius relation [41, 43], and the maximum massive at least 2 $M_\odot$ neutron stars, we derive constraints on the symmetry energy in the density region $\rho_0 - 3\rho_0$. At the saturation density, the symmetry energy is J = 30.66±0.96 MeV and the slope is L = 49.47± 20.39 MeV, which are consistent with the overlap region of $J - L$ constraints from some territory experiments. The symmetry energy constraints at $2\rho_0$ and $3\rho_0$ are $S(2\rho_0)$ = 40.54± 12.47 MeV and $S(3\rho_0)$ = 44.12±29.38 MeV, as shown in Fig. 5.

In the next step, we will explore the entire parameter space of relativistic mean-field models using Bayesian inference with neutron star observational data, which can refine the parameter constraints and provide quantitative constraints on the EoS. Furthermore, the combination of constraints on the EoS from heavy-ion collision analyses (e.g., K^-/K^+ data), neutron star cooling properties such as luminosity data, and measurements of neutron skin thickness in finite nuclei (^{209}Pb and ^{48}Ca) could also reduce the uncertainties of the constraints in future research.

Appendix A

Pressure is plotted as a function of density (ρ/ρ_0) in Fig. 6, which depicts the serval constraints for the pressure, i.e., pressure constraint by the neutron star observables in this paper (blue shadowed region), the experimental flow (orange area) [2], the kaon production (dark purple region) [138], Giant Monopole Resonance (red dashed line) [139], χEFT (magenta hatches) based on the Gaussian Process–BUQEYE Collaboration [10, 136, 137], and the constraint from astronomical observations and nuclear experiments (gray hatched shaded area) [47]. We can observe from Fig .6 that the pressure is within the regions of the kaon production and Giant Monopole Resonance at $\rho_0 \leq \rho \leq 2.2\rho_0$. In addition, the pressure is almost all in the regions of the experimental

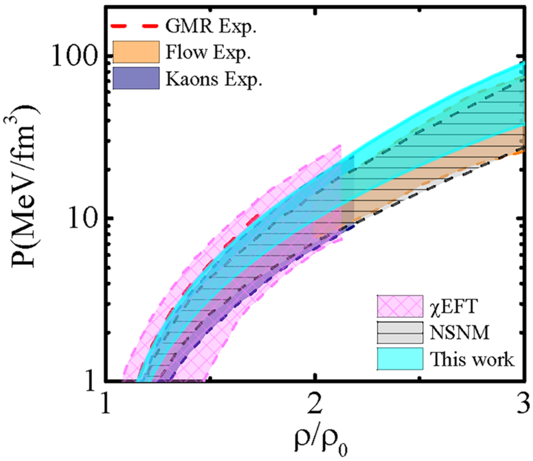

Fig. 6 (Color online) Pressure as a function of density. The light blue shadowed region indicates the pressure constraint by the neutron star observables from this paper, the orange regions are the experimental flow data from Ref. [2], the dark purple region shows data obtained from available kaon production data, the red dashed line presents Giant Monopole Resonance data from Ref. [139], the magenta hatched contours represent the calculations from χEFT based on Gaussian Process from the BUQEYE Collaboration [10, 136, 137], and the gray hatched shaded area shows the constraint from neutron star observations and nuclear matter experiments [47]

flow at a density $\rho > 2.2\rho_0$. Compared with the constraint by the experimental data, we support all regions of the pressure–density region from ρ_0 to $3\rho_0$, which can complement the constraint on the EoS.

Author contributions All authors contributed to the study conception and design. Material preparation, data collection and analysis were performed by YC, YT, C-JX, Y-XZ, and Z-XL. The first draft of the manuscript was written by YC and all authors commented on previous versions of the manuscript. All authors read and approved the final manuscript.

Data availability The data that support the findings of this study are openly available in Science Data Bank at https://cstr.cn/31253.11.sciencedb.j00186.00663 and https://www.doi.org/10.57760/sciencedb.j00186.00663.

Declarations

Conflict of interest The authors declare that they have no conflict of interest.

References

1. B.A. Li, C.M. Ko, W. Bauer, Isospin physics in heavy ion collisions at intermediate-energies. Int. J. Mod. Phys. E **7**, 147 (1998). https://doi.org/10.1142/S0218301398000087
2. P. Danielewicz, R. Lacey, W.G. Lynch, Determination of the equation of state of dense matter. Science **298**, 1592 (2002). https://doi.org/10.1126/science.1078070
3. J.M. Lattimer, M. Prakash, The physics of neutron stars. Science **304**, 536 (2004). https://doi.org/10.1126/science.1090720
4. J.M. Lattimer, M. Prakash, Neutron star observations: prognosis for equation of state constraints. Phys. Rep. **442**(109), 10 (2007). https://doi.org/10.1016/j.physrep.2007.02.003
5. A.W. Steiner, M. Prakash, J.M. Lattimer et al., Isospin asymmetry in nuclei and neutron stars. Phys. Rep. **411**, 325 (2005). https://doi.org/10.1016/j.physrep.2005.02.004
6. V. Baran, M. Colonna, V. Greco et al., Reaction dynamics with exotic beams. Phys. Rep. **410**, 335 (2005). https://doi.org/10.1016/j.physrep.2004.12.004
7. B.A. Li, L.W. Chen, C.M. Ko, Recent progress and new challenges in isospin physics with heavy-ion reactions. Phys. Rep. **464**, 113 (2008). https://doi.org/10.1016/j.physrep.2008.04.005
8. P.G. Reinhard, W. Nazarewicz, Nuclear charge and neutron radii and nuclear matter: trend analysis in Skyrme density-functional-theory approach. Phys. Rev. C **93**, 051303 (2016). https://doi.org/10.1103/PhysRevC.93.051303
9. B.G. Todd-Rutel, J. Piekarewicz, Neutron-rich nuclei and neutron stars: a new accurately calibrated interaction for the study of neutron-rich matter. Phys. Rev. Lett. **95**, 122501 (2005). https://doi.org/10.1103/PhysRevLett.95.122501
10. C. Drischler, R.J. Furnstahl, J.A. Melendez et al., How well do we know the neutron-matter equation of state at the densities inside neutron stars? A Bayesian approach with correlated uncertainties. Phys. Rev. Lett. **125**, 202702 (2020). https://doi.org/10.1103/PhysRevLett.125.202702
11. M.B. Tsang, Y. Zhang, P. Danielewicz et al., Constraints on the density dependence of the symmetry energy. Phys. Rev. Lett. **102**, 122701 (2009). https://doi.org/10.1103/PhysRevLett.102.122701
12. L.W. Chen, C.M. Ko, B.A. Li et al., Density slope of the nuclear symmetry energy from the neutron skin thickness of heavy nuclei. Phys. Rev. C **82**, 024321 (2010). https://doi.org/10.1103/PhysRevC.82.024321
13. L. Trippa, G. Colo, E. Vigezzi, The Giant Dipole Resonance as a quantitative constraint on the symmetry energy. Phys. Rev. C **77**, 061304 (2008). https://doi.org/10.1103/PhysRevC.77.061304
14. A. Tamii, I. Poltoratska, P. von Neumann-Cosel et al., Complete electric dipole response and the neutron skin in 208Pb. Phys. Rev. Lett. **107**, 062502 (2011). https://doi.org/10.1103/PhysRevLett.107.062502
15. X. Roca-Maza, M. Centelles, X. Viñas et al., Electric dipole polarizability in ^{208}Pb: insights from the droplet model. Phys. Rev. C **88**, 024316 (2013). https://doi.org/10.1103/PhysRevC.88.024316
16. T. Kortelainen, M. Lesinski, J. Moré et al., Nuclear energy density optimization. Phys. Rev. C **82**, 024313 (2010). https://doi.org/10.1103/PhysRevC.82.024313
17. A.W. Steiner, J.M. Lattimer, E.F. Brown, The equation of state from observed masses and radii of neutron stars. Astrophys. J. **722**, 33 (2010). https://doi.org/10.1088/0004-637X/722/1/33
18. A.W. Steiner, J.M. Lattimer, E.F. Brown, The neutron star mass-radius relation and the equation of state of dense matter. Astrophys. J. **765**, L5 (2013). https://doi.org/10.1088/2041-8205/765/1/L5
19. P. Danielewicz, P. Singh, J. Lee, Symmetry energy III: Isovector skins. Nucl. Phys. A **958**, 147 (2017). https://doi.org/10.1016/j.nuclphysa.2016.11.008
20. K. Hebeler, J.M. Lattimer, C.J. Pethick et al., Constraints on neutron star radii based on chiral effective field theory interactions. Phys. Rev. Lett. **105**, 161102 (2010). https://doi.org/10.1103/PhysRevLett.105.161102
21. S. Gandolfi, J. Carlson, S. Reddy, The maximum mass and radius of neutron stars and the nuclear symmetry energy. Phys.

Rev. C **85**, 032801(R) (2012). https://doi.org/10.1103/PhysRevC.85.032801
22. I. Tews, J.M. Lattimer, A. Ohnishi et al., Symmetry parameter constraints from a lower bound on neutron-matter energy. Astrophys. J. **848**, 105 (2017). https://doi.org/10.3847/1538-4357/aa8db9
23. M. Thiel, C. Sfienti, J. Piekarewicz et al., Neutron skins of atomic nuclei: per aspera ad astra. J. Phys. G **46**, 093003 (2019). https://doi.org/10.1088/1361-6471/ab2c6d
24. B.T. Reed, F.J. Fattoyev, C.J. Horowitz et al., Implications of PREX-2 on the equation of state of neutron-rich matter. Phys. Rev. Lett. **126**, 172503 (2021). https://doi.org/10.1103/PhysRevLett.126.172503
25. Z. Xiao, B.A. Li et al., Circumstantial evidence for a soft nuclear symmetry energy at suprasaturation densities. Phys. Rev. Lett. **102**, 062502 (2009). https://doi.org/10.1103/PhysRevLett.102.062502
26. M. Zhang, Z.G. Xiao, B.A. Li et al., A Systematic study of the pi-/pi+ ratio in heavy-ion collisions with the same neutron/proton ratio but different masses. Phys. Rev. C **80**, 034616 (2009). https://doi.org/10.1103/PhysRevC.80.034616
27. W.J. Xie, J. Su, L. Zhu et al., Symmetry energy and pion production in the Boltzmann–Langevin approach. Phys. Lett. B **718**, 1510 (2013). https://doi.org/10.1016/j.physletb.2012.12.021
28. Z.Q. Feng, G.M. Jin, Probing high-density behavior of symmetry energy from pion emission in heavy-ion collisions. Phys. Lett. B **683**, 140 (2010). https://doi.org/10.1016/j.physletb.2009.12.006
29. J. Xu, C.M. Ko, Y. Oh, Isospin-dependent pion in-medium effects on charged pion ratio in heavy ion collisions. Phys. Rev. C **81**, 024910 (2010). https://doi.org/10.1103/PhysRevC.81.024910
30. M.D. Cozma, The impact of energy conservation in transport models on the π^-/π^+ multiplicity ratio in heavy-ion collisions and the symmetry energy. Phys. Lett. B **753**, 166 (2016). https://doi.org/10.1016/j.physletb.2015.12.015
31. T. Song, C.M. Ko, Modifications of the pion-production threshold in the nuclear medium in heavy ion collisions and the nuclear symmetry energy. Phys. Rev. C **91**, 014901 (2015). https://doi.org/10.1103/PhysRevC.91.014901
32. P. Russotto, P.Z. Wu, M. Zoric et al., Symmetry energy from elliptic flow in ^{197}Au+^{197}Au. Phys. Lett. B **697**, 471 (2011). https://doi.org/10.1016/j.physletb.2011.02.033
33. M.D. Cozma, Y. Leifels, W. Trautmann et al., Toward a model-independent constraint of the high-density dependence of the symmetry energy. Phys. Rev. C **88**, 044912 (2013). https://doi.org/10.1103/PhysRevC.88.044912
34. H.T. Cromartie, E. Fonseca, S.M. Ransom et al., Relativistic Shapiro delay measurements of an extremely massive millisecond pulsar. Nat. Astron. **4**, 72–76 (2019). https://doi.org/10.1038/s41550-019-0880-2
35. E. Fonseca, H.T. Cromartie, T.T. Pennucci et al., Refined mass and geometric measurements of the high-mass PSR J0740+6620. Astrophys. J. Lett. **915**, L12 (2021). https://doi.org/10.3847/2041-8213/ac03b8
36. R. Abbott, T.D. Abbott, S. Abraham et al., (LIGO Scientifc, Virgo), GW190814: gravitational waves from the coalescence of a 23 solar mass black hole with a 2.6 solar mass compact object. Astrophys. J. Lett. **896**, L44 (2020). https://doi.org/10.3847/2041-8213/ab960f
37. B.A. Li, P.G. Krastev, D.H. Wen et al., Towards understanding astrophysical effects of nuclear symmetry energy. Eur. Phys. J. A **55**, 117 (2019). https://doi.org/10.1140/epja/i2019-12780-8
38. F.J. Fattoyev, C.J. Horowitz, J. Piekarewicz et al., GW190814: impact of a 2.6 solar mass neutron star on the nucleonic equations of state. Phys. Rev. C **102**, 065805 (2020). https://doi.org/10.1103/PhysRevC.102.065805
39. M. Miller, F.K. Lamb, A.J. Dittmann et al., The radius of PSR J0740+6620 from NICER and XMM-Newton data. Astrophys. J. **918**, L28 (2021). https://doi.org/10.3847/2041-8213/ac089b
40. S.P. Tang, J.L. Jiang, M.Z. Han et al., Constraints on the phase transition and nuclear symmetry parameters from PSR J0740+6620 and multimessenger data of other neutron stars. Phys. Rev. D **104**, 063032 (2021). https://doi.org/10.1103/PhysRevD.104.063032
41. B.P. Abbott, R. Abbott, T.D. Abbott et al., Properties of the binary neutron star merger GW170817. Phys. Rev. X **9**, 011001 (2019). https://doi.org/10.1103/PhysRevX.9.011001
42. B.P. Abbott, R. Abbott, T.D. Abbott et al., GW170817: measurements of neutron star radii and equation of state. Phys. Rev. Lett. **121**, 161101 (2018). https://doi.org/10.1103/PhysRevLett.121.161101
43. M.C. Miller, F.K. Lamb, A.J. Dittmann et al., PSR J0030+0451 mass and radius from NICER data and implications for the properties of neutron star matter. Astrophys. J. Lett. **887**, L24 (2019). https://doi.org/10.3847/2041-8213/ab50c5
44. W.J. Xie, B.A. Li, Bayesian inference of the symmetry energy of superdense neutron-rich matter from future radius measurements of massive neutron stars. Astrophys. J. Lett. **899**, 4 (2020). https://doi.org/10.3847/1538-4357/aba271
45. Y.X. Zhang, M. Liu, C.J. Xia et al., Constraints on the symmetry energy and its associated parameters from nuclei to neutron stars. Phys. Rev. C **101**, 034303 (2020). https://doi.org/10.1103/PhysRevC.101.034303
46. S.K. Greif, K. Hebeler, J.M. Lattimer et al., Equation of state constraints from nuclear physics, neutron star masses, and future moment of inertia measurements. Astrophys. J. Lett. **901**, 155 (2020). https://doi.org/10.3847/1538-4357/abaf55
47. C.Y. Tsang, M.B. Tsang, W.G. Lynch et al., Determination of the equation of state from nuclear experiments and neutron star observations. Nat. Astron. **8**, 328 (2024). https://doi.org/10.1038/s41550-023-02161-z
48. C.Y. Tsang, M.B. Tsang, P. Danielewicz et al., Insights on Skyrme parameters from GW170817. Phys. Lett. B **796**, 1–5 (2019). https://doi.org/10.1016/j.physletb.2019.05.055
49. B.A. Li, B.J. Cai, W.J. Xie et al., Progress in constraining nuclear symmetry energy using neutron star observables since GW170817. Universe **7**, 182 (2021). https://doi.org/10.3390/universe7060182
50. C.Y. Tsang, M.B. Tsang, P. Danielewicz et al., Impact of the neutron-star deformability on equation of state parameters. Phys. Rev. C **102**, 045808 (2020). https://doi.org/10.1103/PhysRevC.102.045808
51. P.G. Reinhard, The relativistic mean field description of nuclei and nuclear dynamics. Rep. Prog. Phys. **52**, 439 (1989). https://doi.org/10.1088/0034-4885/52/4/002
52. P. Ring, Relativistic mean field in finite nuclei. Prog. Part. Nucl. Phys. **37**, 193 (1996). https://doi.org/10.1016/0146-6410(96)00054-3
53. M. Dutra, O. Lourenço, S.S. Avancini et al., Relativistic mean-field hadronic models under nuclear matter constraints. Phys. Rev. C **90**, 055203 (2014). https://doi.org/10.1103/PhysRevC.90.055203
54. B.D. Serot, J.D. Walecka, Recent progress in quantum hadrodynamics. Int. J. Mod. Phys. E **6**, 515 (1997). https://doi.org/10.1142/S0218301397000299
55. T. Bürvenich, D.G. Madland, J.A. Maruhn et al., Nuclear ground state observables and QCD scaling in a refined relativistic point coupling model. Phys. Rev. C **65**, 044308 (2002). https://doi.org/10.1103/PhysRevC.65.044308

56. C. Fuchs, H. Lenske, H.H. Wolter, Density dependent hadron field theory. Phys. Rev. C **52**, 3043 (1995). https://doi.org/10.1103/PhysRevC.52.3043
57. J.J. Rusnak, R.J. Furnstahl, Relativistic point coupling models as effective theories of nuclei. Nucl. Phys. A **627**, 495 (1997). https://doi.org/10.1016/S0375-9474(97)00598-8
58. G.A. Lalazissis, T. Nikšić, D. Vretenar et al., New relativistic mean-field interaction with density-dependent meson–nucleon couplings. Phys. Rev. C **71**, 024312 (2005). https://doi.org/10.1103/PhysRevC.71.024312
59. X. Roca-Maza, X. Viñas, M. Centelles et al., Relativistic mean field interaction with density dependent meson–nucleon vertices based on microscopical calculations. Phys. Rev. C **84**, 054309 (2011). https://doi.org/10.1103/PhysRevC.84.054309
60. J. Piekarewicz, Correlating the giant monopole resonance to the nuclear matter incompressibility. Phys. Rev. C **66**, 034305 (2002). https://doi.org/10.1103/PhysRevC.66.034305
61. M. Rufa, P.G. Reinhard, J.A. Maruhn et al., Optimal parametrization for the relativistic mean-field model of the nucleus. Phys. Rev. C **38**, 390 (1988). https://doi.org/10.1103/PhysRevC.38.390
62. G.A. Lalazissis, J. Karatzikos, P. Ring, A New parametrization for the Lagrangian density of relativistic mean field theory. Phys. Rev. C **55**, 540 (1997). https://doi.org/10.1103/PhysRevC.55.540
63. G.A. Lalazissis, S. Karatzikos, R. Fossion et al., The effective force NL3 revisited. Phys. Lett. B **671**, 36 (2009). https://doi.org/10.1016/j.physletb.2008.11.070
64. B. Nerlo-Pomoroska, J. Sykut, A New parameter set for the relativistic mean field theory. Int. J. Mod. Phys. E **13**, 75 (2004). https://doi.org/10.1142/S0218301304001758
65. M. Rashdan, Structure of exotic nuclei and superheavy elements in a relativistic shell model. Phys. Rev. C **63**, 044303 (2001). https://doi.org/10.1103/PhysRevC.63.044303
66. P.G. Reinhard, The nonlinearity of the scalar field in a relativistic mean-field theory of the nucleus. Z. Phys. A **329**, 257 (1988). https://doi.org/10.1007/BF01290231
67. A. Sulaksono, T. Mart, C. Bahri, Nilsson parameters kappa and mu in the relativistic mean field models. Phys. Rev. C **71**, 034312 (2005). https://doi.org/10.1103/PhysRevC.71.034312
68. N.K. Glendenning, *Compact Stars: Nuclear Physics, Particle Physics, and General Relativity*, 2nd edn. (Springer, New York, 2000)
69. N.K. Glendenning, The hyperon composition Of neutron stars. Phys. Lett. B **114**, 392 (1982). https://doi.org/10.1016/0370-2693(82)90078-8
70. N.K. Glendenning, S.A. Moszkowski, Reconciliation of neutron star masses and binding of the lambda in hypernuclei. Phys. Rev. Lett. **67**, 2414 (1991). https://doi.org/10.1103/PhysRevLett.67.2414
71. S.K. Ghosh, S.C. Phatak, P.K. Sahu, Quark hadron phase transition and hybrid stars. Z. Phys. A **352**, 457 (1995). https://doi.org/10.1007/BF01299764
72. B. Liu, H. Guo, M. Di Toro et al., Neutron stars with the isovector scalar field. Eur. Phys. J. A **25**, 293 (2005). https://doi.org/10.1140/epja/i2005-10095-1
73. A.A. Dadi, Parametrization of the relativistic $(\sigma - \omega)$ model for nuclear matter. Phys. Rev. C **82**, 025203 (2010). https://doi.org/10.1103/PhysRevC.82.025203
74. R.J. Furnstahl, B.D. Serot, H.B. Tang, A chiral effective Lagrangian for nuclei. Nucl. Phys. A **615**, 441 (1997). https://doi.org/10.1016/S0375-9474(96)00472-1
75. S. Gmuca, Finite-nuclei calculations based on relativistic mean-field effective interactions. Nucl. Phys. A **547**, 447 (1992). https://doi.org/10.1016/0375-9474(92)90032-F
76. C.J. Horowitz, J. Piekarewicz, Neutron star structure and the neutron radius of Pb-208. Phys. Rev. Lett. **86**, 5647 (2001). https://doi.org/10.1103/PhysRevLett.86.5647
77. M. Centelles, X. Vinas, M. Barranco et al., Semiclassical approximations in nonlinear sigma omega models. Nucl. Phys. A **537**, 486 (1992). https://doi.org/10.1016/0375-9474(92)90365-Q
78. J.K. Bunta, S. Gmuca, Asymmetric nuclear matter in the relativistic mean field approach with vector cross interaction. Phys. Rev. C **68**, 054318 (2003). https://doi.org/10.1103/PhysRevC.68.054318
79. H. Müller, B.D. Serot, Phase transitions in warm, asymmetric nuclear matter. Phys. Rev. C **52**, 2072 (1995). https://doi.org/10.1103/PhysRevC.52.2072
80. F.J. Fattoyev, J. Piekarewicz, Relativistic models of the neutron-star matter equation of state. Phys. Rev. C **82**, 025805 (2010). https://doi.org/10.1103/PhysRevC.82.025805
81. M.M. Sharma, A.R. Farhan, S. Mythili, Shell effects in nuclei with vector selfcoupling of omega meson in relativistic Hartree–Bogolyubov theory. Phys. Rev. C **61**, 054306 (2000). https://doi.org/10.1103/PhysRevC.61.054306
82. Y. Sugahara, H. Toki, Relativistic mean field theory for unstable nuclei with nonlinear sigma and omega terms. Nucl. Phys. A **579**, 557 (1994). https://doi.org/10.1016/0375-9474(94)90923-7
83. W. Long, J. Meng, N. VanGiai et al., New effective interactions in RMF theory with nonlinear terms and density dependent meson nucleon coupling. Phys. Rev. C **69**, 034319 (2004). https://doi.org/10.1103/PhysRevC.69.034319
84. J. Piekarewicz, M. Centelles, Incompressibility of neutron-rich matter. Phys. Rev. C **79**, 054311 (2009). https://doi.org/10.1103/PhysRevC.79.054311
85. A. Sulaksono, T. Mart, Low densities instability of relativistic mean field models. Phys. Rev. C **74**, 045806 (2006). https://doi.org/10.1103/PhysRevC.74.045806
86. B.K. Agrawal, Asymmetric nuclear matter and neutron-skin in extended relativistic mean field model. Phys. Rev. C **81**, 034323 (2010). https://doi.org/10.1103/PhysRevC.81.034323
87. J. Piekarewicz, S.P. Weppner, Insensitivity of the elastic proton-nucleus reaction to the neutron radius of Pb-208. Nucl. Phys. A **778**, 10 (2006). https://doi.org/10.1016/j.nuclphysa.2006.08.004
88. R. Kumar, B.K. Agrawal, S.K. Dhiman, Effects of omega meson self-coupling on the properties of finite nuclei and neutron stars. Phys. Rev. C **74**, 034323 (2006). https://doi.org/10.1103/PhysRevC.74.034323
89. F.J. Fattoyev, C.J. Horowitz, J. Piekarewicz et al., Relativistic effective interaction for nuclei, giant resonances, and neutron stars. Phys. Rev. C **82**, 055803 (2010). https://doi.org/10.1103/PhysRevC.82.055803
90. C.J. Horowitz, J. Piekarewicz, Constraining URCA cooling of neutron stars from the neutron radius of Pb-208. Phys. Rev. C **66**, 055803 (2002). https://doi.org/10.1103/PhysRevC.66.055803

91. M. DelEstal, M. Centelles, X. Viñas et al., Effects of new nonlinear couplings in relativistic effective field theory. Phys. Rev. C **63**, 024314 (2001). https://doi.org/10.1103/PhysRevC.63.024314
92. S.K. Dhiman, R. Kumar, B.K. Agrawal, Non-rotating and rotating neutron stars in the extended field theoretical model. Phys. Rev. C **76**, 045801 (2007). https://doi.org/10.1103/PhysRevC.76.045801
93. M.M. Sharma, Scalar-vector Lagrangian without nonlinear self-interactions of bosonic fields in the relativistic mean-field theory. Phys. Lett. B **666**, 140 (2008). https://doi.org/10.1016/j.physletb.2008.07.005
94. M.M. Haidari, M.M. Sharma, Sigma-omega meson coupling and properties of nuclei and nuclear matter. Nucl. Phys. A **803**, 159 (2008). https://doi.org/10.1016/j.nuclphysa.2008.02.296
95. S. Typel, H.H. Wolter, Relativistic mean field calculations with density dependent meson nucleon coupling. Nucl. Phys. A **656**, 331 (1999). https://doi.org/10.1016/S0375-9474(99)00310-3
96. T. Nikšić, D. Vretenar, P. Finelli et al., Relativistic Hartree–Bogolyubov model with density dependent meson nucleon couplings. Phys. Rev. C **66**, 024306 (2002). https://doi.org/10.1103/PhysRevC.66.024306
97. S. Typel, Relativistic model for nuclear matter and atomic nuclei with momentum-dependent self-energies. Phys. Rev. C **71**, 064301 (2005). https://doi.org/10.1103/PhysRevC.71.064301
98. T. Klähn, D. Blaschke, S. Typel et al., Constraints on the high-density nuclear equation of state from the phenomenology of compact stars and heavy-ion collisions. Phys. Rev. C **74**, 035802 (2006). https://doi.org/10.1103/PhysRevC.74.035802
99. S. Typel, G. Röpke, T. Klähn et al., Composition and thermodynamics of nuclear matter with light clusters. Phys. Rev. C **81**, 015803 (2010). https://doi.org/10.1103/PhysRevC.81.015803
100. G. Baym, C. Pethick, P. Sutherland, The Ground state of matter at high densities: equation of state and stellar models. Astrophys. J. **170**, 299 (1971). https://doi.org/10.1086/151216
101. B. Link, R.I. Epstein, J.M. Lattimer, Pulsar constraints on neutron star structure and equation of state. Phys. Rev. Lett. **83**, 3362 (1999). https://doi.org/10.1103/PhysRevLett.83.3362
102. J. Carriere, C.J. Horowitz, J. Peikarewicz, Low mass neutron stars and the equation of state of dense matter. Astrophys. J. **593**, 463 (2003). https://doi.org/10.1086/376515
103. C. Ducoin, J. Margueron, C. Providência et al., Core-crust transition in neutron stars: predictivity of density developments. Phys. Rev. C **83**, 045810 (2011). https://doi.org/10.1103/PhysRevC.83.045810
104. F. Weber, Strange quark matter and compact stars. Prog. Part. Nucl. Phys. **54**, 193 (2005). https://doi.org/10.1016/j.ppnp.2004.07.001
105. A. Li, G.F. Burgio, U. Lombardo et al., Exotic phases in neutron stars. Int. J. Mod. Phys. E **17**, 1635 (2008). https://doi.org/10.1142/S0218301308010659
106. M. Orsaria, H. Rodrigues, F. Weber et al., Quark deconfinement in high-mass neutron stars. Phys. Rev. C **89**, 015806 (2014). https://doi.org/10.1103/PhysRevC.89.015806
107. A. Gal, E.V. Hungerford, D.J. Millener, Strangeness in nuclear physics. Rev. Mod. Phys. **88**(3), 035004 (2016). https://doi.org/10.1103/RevModPhys.88.035004
108. L. Tolos, L. Fabbietti, Strangeness in nuclei and neutron stars. Prog. Part. Nucl. Phys. **112**, 103770 (2020). https://doi.org/10.1016/j.ppnp.2020.103770
109. M. Oertel, M. Hempel, T. Klähn et al., Equations of state for supernovae and compact stars. Rev. Mod. Phys. **89**(1), 015007 (2017). https://doi.org/10.1103/RevModPhys.89.015007
110. A. Li, F. Huang, R.X. Xu, Too massive neutron stars: the role of dark matter? Astropart. Phys. **37**, 70 (2012). https://doi.org/10.1016/j.astropartphys.2012.07.006
111. H.S. Sahoo, G. Mitra, R. Mishra et al., Neutron star matter with Δ isobars in a relativistic quark model. Phys. Rev. C **98**, 045801 (2018). https://doi.org/10.1103/PhysRevC.98.045801
112. H.C. Das, A. Kumar, B. Kumar et al., Effects of dark matter on the nuclear and neutron star matter. Mon. Not. Roy. Astron. Soc. **495**, 4893 (2020). https://doi.org/10.1093/mnras/staa1435
113. D. Lonardoni, A. Lovato, S. Gandolfi et al., Hyperon puzzle: hints from quantum Monte Carlo calculations. Phys. Rev. Lett. **114**, 092301 (2015). https://doi.org/10.1103/PhysRevLett.114.092301
114. Z.Q. Feng, Extracting the hyperon–nucleon interaction via collective flows in heavy-ion collisions. Phys. Lett. B **851**, 138580 (2024). https://doi.org/10.1016/j.physletb.2024.138580
115. S.N. Wei, Z.Q. Feng, W.Z. Jiang, Correlation of the hyperon potential stiffness with hyperon constituents in neutron stars and heavy-ion collisions. Phys. Lett. B **853**, 138658 (2024). https://doi.org/10.1016/j.physletb.2024.138658
116. J.S. Read, B.D. Lackey, B.J. Owen et al., Constraints on a phenomenologically parameterized neutron-star equation of state. Phys. Rev. D. **79**, 124032 (2009). https://doi.org/10.1103/PhysRevD.79.124032
117. J.M. Lattimer, M. Prakash, The equation of state of hot, dense matter and neutron stars. Phys. Rep. **621**, 127 (2016). https://doi.org/10.1016/j.physrep.2015.12.005
118. F.J. Fattoyev, J. Carvajal, W.G. Newton et al., Constraining the high-density behavior of the nuclear symmetry energy with the tidal polarizability of neutron stars. Phys. Rev. C **87**, 015806 (2013). https://doi.org/10.1103/PhysRevC.87.015806
119. R.C. Tolman, *Relativity, Thermodynamics and Cosmology* (Oxford University Press, Oxford, 1934)
120. R.C. Tolman, Static solutions of Einstein's field equations for spheres of fluid. Phys. Rev. **55**, 364 (1939). https://doi.org/10.1103/PhysRev.55.364
121. J.R. Oppenheimer, G.M. Volkoff, On massive neutron cores. Phys. Rev. **55**, 374 (1939). https://doi.org/10.1103/PhysRev.55.374
122. T. Damour, A. Nagar, Relativistic tidal properties of neutron stars. Phys. Rev. D **80**, 084035 (2009). https://doi.org/10.1103/PhysRevD.80.084035
123. T. Hinderer, B.D. Lackey, R.N. Lang et al., Tidal deformability of neutron stars with realistic equations of state and their gravitational wave signatures in binary inspiral. Phys. Rev. D **81**, 123016 (2010). https://doi.org/10.1103/PhysRevD.81.123016
124. S. Postnikov, M. Prakash, J.M. Lattimer, Tidal love numbers of neutron and self-bound quark stars. Phys. Rev. D **82**, 024016 (2010). https://doi.org/10.1103/PhysRevD.82.024016
125. R.J. Furnstahl, Neutron radii in mean field models. Nucl. Phys. A **706**, 85 (2002). https://doi.org/10.1016/S0375-9474(02)00867-9
126. C. Ducoin, J. Margueron, C. Providencia, Nuclear symmetry energy and core-crust transition in neutron stars: a critical study. Europhys. Lett. **91**, 32001 (2010). https://doi.org/10.1209/0295-5075/91/32001
127. Z. Zhang, L.W. Chen, Constraining the symmetry energy at subsaturation densities using isotope binding energy difference and

neutron skin thickness. Phys. Lett. B **726**, 234 (2013). https://doi.org/10.1016/j.physletb.2013.08.002
128. C.J. Horowitz, E.F. Brown, Y. Kim et al., A way forward in the study of the symmetry energy: experiment, theory, and observation. J. Phys. G **41**, 093001 (2014). https://doi.org/10.1088/0954-3899/41/9/093001
129. T. Malik, M. Ferreira, B.K. Agrawal et al., Relativistic description of dense matter equation of state and compatibility with neutron star observables: a Bayesian approach. Astrophys. J. **930**, 17 (2022). https://doi.org/10.3847/1538-4357/ac5d3c
130. J.M. Lattimer, A.W. Steiner, Constraints on the symmetry energy using the mass-radius relation of neutron stars. Eur. Phys. J. A **50**, 40 (2014). https://doi.org/10.1140/epja/i2014-14040-y
131. J.M. Lattimer, Y. Lim, Constraining the symmetry parameters of the nuclear interaction. Astrophys. J. **771**, 51 (2013). https://doi.org/10.1088/0004-637X/771/1/51
132. L.W. Chen, C.M. Ko, B.A. Li, Isospin-dependent properties of asymmetric nuclear matter in relativistic mean-field models. Phys. Rev. C **76**, 054316 (2007). https://doi.org/10.1103/PhysRevC.76.054316
133. B.A. Brown, Constraints on the skyrme equations of state from properties of doubly magic nuclei. Phys. Rev. Lett. **111**, 232502 (2013). https://doi.org/10.1103/PhysRevLett.111.232502
134. P. Danielewicz, J. Lee, Symmetry energy II: isobaric analog states. Nucl. Phys. A **922**, 1–70 (2014). https://doi.org/10.1016/j.nuclphysa.2013.11.005
135. Z. Zhang, L.W. Chen, Constraining the density slope of nuclear symmetry energy at subsaturation densities using electric dipole polarizability in ^{208}Pb. Phys. Rev. C **90**, 064317 (2014). https://doi.org/10.1103/PhysRevC.90.064317
136. C. Drischler, K. Hebeler, A. Schwenk, Chiral interactions up to next-to-next-to-next-to-leading order and nuclear saturation. Phys. Rev. Lett. **122**, 042501 (2019). https://doi.org/10.1103/PhysRevLett.122.042501
137. C. Drischler, J.A. Melendez, R.J. Furnstahl et al., Quantifying uncertainties and correlations in the nuclear-matter equation of state. Phys. Rev. C **102**, 054315 (2020). https://doi.org/10.1103/PhysRevC.102.054315
138. W.G. Lynch, M.B. Tsang, Y. Zhang et al., Probing the symmetry energy with heavy ions. Prog. Part. Nucl. Phys. **62**, 427 (2009). https://doi.org/10.1016/j.ppnp.2009.01.001
139. D.H. Youngblood, H.L. Clark, Y.W. Lui, Incompressibility of Nuclear Matter from the Giant Monopole Resonance. Phys. Rev. Lett. **82**, 691 (1999). https://doi.org/10.1103/PhysRevLett.82.691